HYDROGEN GAS GENERATION BY WATER VAPOR DISSOCIATION IN AN Al/Al_2O_3 MICROCHANNEL PLASMA DEVICE

BY

ZHEN DAI

THESIS

Submitted in partial fulfillment of the requirements
for the degree of Master of Science in Electrical and Computer Engineering
in the Graduate College of the
University of Illinois at Urbana-Champaign, 2015

Urbana, Illinois

Advisor:

Professor J. Gary Eden

ABSTRACT

An aluminum/alumina (Al/Al_2O_3) microchannel plasma reactor is used to generate H_2 with an energy efficiency of 2.5 % by dissociating water vapor in Ar at atmospheric pressure and room temperature. The value compares favorably to other plasma reactors reported in the literature, having reported energy efficiencies ≤ 2 %. Additionally, spectra of the H_α line are used to calculate electron densities, which are in the vicinity of $1.5 \pm 0.2 \times 10^{16}$ cm^{-3}, while spectra of the OH(A-X) transition show a distinctly non-equilibrium population distribution in the OH($A^2\Sigma^+$) state. Al/Al_2O_3 microchannel plasma device was shown to be efficient in water dissociation as compared with other plasma reactors recently reported in the literature.

ACKNOWLEDGMENTS

I wish to express sincere appreciation to Professors Gary Eden and Sung-Jin Park for their scintillating wisdom and effulgent kindness in guiding this thesis work. In addition, Thomas Galvin's and Thomas Houlahan's protean intellects and endless capacities for work have inspired me intellectually and aided the physical construction of many experiments. Moreover, Chul Shin and Teagon Oh's foundational work on the gas flow system was imperative to the experiments, especially the early ones. Finally, I'd like to thank my family and my boyfriend, Jingshu Zhang, whose support and encouragement, fairer than the Orphic lyre, comforted my frail thoughts over whelming seas and sounding hills.

TABLE OF CONTENTS

CHAPTER 1

INTRODUCTION

The depletion of conventional fossil fuels coupled with their severe environmental effects such as greenhouse gases and particulate emission demand a cleaner, more sustainable energy source [1]. The use of hydrogen gas (H_2) as a carbon-free energy source, or the transition to a hydrogen economy, is considered an important method to alleviate the environmental and social strain caused by traditional fuel sources [2]. Although H is the most abundant element on earth, H_2 does not exist naturally and must be artificially produced. Traditionally, H_2 is produced from steam methane reforming, coal gasification and electrolysis [3]. Dissociating water through plasma-chemical reactions has several advantages such as high specific productivities [4], low limitations on diffusion speed of the neutral molecules [5] and carbon-neutrality.

Some research has been conducted aiming at generating H_2 from water vapor through plasma-chemical reactions. Chen *et al.* [6] used tubular plasma and catalyst reactors with gold as a catalyst to dissociate water vapor carried by a stream of Ar. They achieved a dissociation degree of 14% and highest energy efficiency of around 2%. In a study conducted by Luo *et al.* [7], an energy efficiency of 1.1% was achieved without adopting a Pt catalyst. Kabashima *et al.* [8] used a packed-bed plasma reactor to dissociate a stream of water vapor carried by N_2. They achieved 63% of water dissociation but at a low energy efficiency << 1%. Nguyen *et al.* [9] dissociated water vapor carried by Ar

using a microwave plasma and achieved an energy efficiency of about 0.1% while producing 23 sccm of H_2.

In this study, microchannel plasma devices have been used to produce hydrogen gas from water vapor carried by Ar. Previous studies have shown that aluminum/ alumina microchannel plasma reactors were capable of efficiently synthesizing ozone gas at atmospheric pressure and room temperature [10]. Using a similar reactor, H_2 was generated from a mixture of water vapor and Ar at room temperature and atmospheric pressure with dissociation efficiencies higher than those currently found in the literature.

CHAPTER 2

EXPERIMENTAL

The fabrication processes of the plasma chemical reactors were described in detail in our previous publications [10]–[12]. The device structure used in this study was similar to the Al/Al_2O_3 device described in Ref. 10 with the exception that a single anodization step was used to produce the Al/Al_2O_3 substrate. A schematic of the device structure is shown in Figure 1. The fabrication process is briefly summarized as follows. A piece of 500 μm thick aluminum foil was anodized in a 0.3 M oxalic acid solution for 48 hours at 100 V and room temperature. The result of this was a layer of nanoporous alumina grown on the native aluminum, making the entire substrate about 680 μm thick. A second aluminum sheet with an initial thickness of 125 μm was anodized for 4 hours under the same conditions and used as the top electrode. The alumina layer produced this way was approximately 40 μm thick. A polydimethylsiloxane (PDMS) stamp was used as a photolithographic mask to define the geometry of the microchannels. It was molded from a silicon master stamp fabricated with conventional photolithographic processes. The PDMS stamp was pressed into a UV-curable polymer applied on top of the alumina layer, which was subsequently cured to expose only the channel areas. The channels were then etched with a micropowder blaster for which the speed, working distance to the substrate, nozzle geometry, backing pressure, and number of repetitions for blasting were controlled by a computer. The resulting geometry was an array of 12 channels 250 μm in width, 150 μm in depth, 3 cm in length and with a 500 μm periodicity.

Following the etching steps, the top electrode and bottom channel layer were hermetically sealed. Two glass tubes serving as the gas inlet and outlet were also hermetically attached at the ends of the channels. Water vapor was introduced into the device through a bubbler using ultra-high purity Ar as the carrier gas at room temperature and atmospheric pressure. A similar method was used in Ref. 6. The resulting feed gas contained 2.3 mol % of water vapor according to the equilibrium vapor pressure of water. A schematic of the gas flow and testing system setup is shown in Figure 2. The Ar gas flow was controlled by a calibrated Brooks UFC-1660 mass flow controller (MFC) with ±10 sccm accuracy. The device was driven by a 20 kHz sinusoidal wave at controllable voltages to excite plasmas in the channel region. The effluent gas composition was analyzed in-line by an Inficon Transpector 2.0 residual gas analyzer (RGA). To obtain quantitative H_2 concentration information, the RGA was calibrated with known flow rates of Ar and H_2 gases to obtain a calibration factor relating the current signal response for H_2 and Ar as measured by the RGA. During the actual calculation, the mole percentage of Ar in the effluent was assumed to be constant because its molar concentration change was < 0.2 %.

The emission spectrum of the plasma was recorded using a Princeton Instrument PIMAX 4 gated intensified charge-coupled device (ICCD) camera coupled with an Acton SP2570 0.75 m Czerny-Turner monochromator. The spectral resolution of this system was calibrated with known atomic lines at various wavelengths. For devices that were used to collect the spectra, a sapphire window was embedded in the gas inlet tube so that the UV portion of the spectra could be transmitted.

The absolute yield of hydrogen gas (Y_H) was calculated based on the equation:

$$Y_H = \frac{S_H}{C \times S_{Ar}} \times Q_{Ar} \quad (1)$$

where S_H and S_{Ar} were the current signal strengths detected by the RGA from the peaks with masses 2 and 40, corresponding to H_2 and Ar. C was the calibration factor. Q_{Ar} was the flow rate of Ar. The energy efficiency of water dissociation (η) was calculated based on:

$$\eta = Y_H \times \frac{H_{H_2O}}{P} \quad (2)$$

where H_{H_2O} was the higher heating value of water (142.18 MJ/kg), and P was the discharge power.

CHAPTER 3

RESULTS AND DISCUSSION

The absolute conversion rate of H_2 as a function of the input power for Ar flow rates ranging from 20 sccm to 900 sccm is plotted in Figure 3. The maximum H_2 production rate achieved in this experiment was ~ 28 sccm recorded at the maximum flow rate and discharge power. For all flow rates, there existed an input power level below which no hydrogen was generated. In this particular system, this power was found to be ~ 0.5 W through linear regression. In a water vapor plasma, such a dissociation threshold indicated the existence of an activation barrier to the formation of H_2 gas [4]. In addition, the H_2 production rate rose linearly with the discharge power at a constant Ar flow rate. This increase was likely due to a higher density of the reactive intermediate species as indicated by the increased intensity in the optical emission spectra (OES).

The effect of power on the H_2 production rate, as measured by the gradient in the linear regression shown in Figure 3, differed for varying Ar flow rates. Since the flow rate was observed to have little effect on the threshold dissociation power, an increase in the gradient indicated a higher energy efficiency for H_2 production. The relationship between this production efficiency and the Ar flow rate is plotted in Figure 4. At low Ar flow rates of up to 300 sccm, the production efficiency rose nearly linearly with the flow rate. Beyond that level, the efficiency continued to increase, but with a decreasing rate, eventually leveling at about 5.8 sccm/W. As the water vapor concentration was constant at all Ar flow rates, the dissociation degree of water then decreased throughout this

region with no gain in absolute H_2 production, indicating the existence of an optimal flow rate for this system. There were several reasons that might account for this saturation. In terms of chemical equilibrium, the reverse recombination reaction was in constant competition with the forward dissociation reaction. As the flow increased from a small value, even though the absolute H_2 production rate increased, the dissociation degree decreased, favoring the forward reaction and therefore increasing the production efficiency. However, at high flow rates, the residence time of the gaseous species in the plasma region became short, reaching ~ 0.5 ms at 900 sccm. This was comparable to the lifetime of some stable reaction intermediates such as OH [13], which participated in the overall reaction through neutral-neutral interaction, charge transfer, and dissociative attachment processes. In addition, previous kinetic studies of water vapor plasmolysis at atmospheric pressure showed that the reaction time scale for reaching equilibrium was on the order of a few milliseconds [14]. It was therefore highly likely that the short residence time was preventing the reaction from reaching equilibrium and thus lowering the dissociation degree.

Another important metric in measuring the effectiveness of H_2 production was energy efficiency, which is plotted in Figure 5 as a function discharge power for various flow rates. At all the tested flow rates, the energy efficiency initially increased with the discharge power at low power levels. However, above ~ 4 W, the energy efficiency reached a maximum level and slowly decreased at higher discharge power, indicating the existence of an optimal power loading. The maximal power efficiency obtained in these experiments was about 2.5% with an Ar flow rate of 900 sccm. Similar trends for various dissociation pathways were described in the literature, where kinetics studies suggested

an optimal discharge power in terms of energy efficiency [15]. In addition, the system impedance increased at high discharge power due to an increase in the reactor temperature, resulting in a decrease in the energy efficiency.

In addition to analyzing the effluent composition, *in situ* diagnostics were capable of providing further insight into relevant kinetic processes occurring within the reactor plasma. In this case, optical emission spectra (OES) served as an excellent *in situ* diagnostic tool. Atomic hydrogen generated in the plasma was a convenient tool for determining the electron density by considering Stark broadening in the emission spectra. H_α spectra were collected with the grating-coupled gated ICCD camera for selected discharge powers near the power level that resulted in the highest energy efficiency at an Ar flow rate of 40 sccm. An example H_α profile is shown in Figure 6. In general, the H_α line full-width at half maximum (FWHM) was considered to be the convolution between a Gaussian component and a Lorentzian component, which resulted in a Voigt profile [16]. The Gaussian component accounted for the effect of Doppler broadening and instrumental broadening, and the Lorentzian component accounted for the effect of collisional broadening and Stark broadening. Following the methods described in Ref. 16, the Doppler broadening was estimated to be 0.008 nm. The collisional broadening was calculated to be 0.09 nm for a gas temperature of 300 K at atmospheric pressure [17]. The instrumental broadening was estimated from an Ar atomic line at 488 nm to be 0.06 nm. The Stark broadening was then fitted as a parameter in the Voigt profile. The resulting electron density based on the fitting routine developed by Gigosis *et al.* [18] was estimated to be $1.5 \pm 0.2 \times 10^{16}/\text{cm}^3$. Here the error represented the uncertainty in the Stark broadening fitting parameter. This electron density was typical of a microplasma

device [19]. Figure 7 shows the estimated electron density as well as the normalized H_α line peak intensity as a function of the discharge power. For the four discharge powers that were examined, there was little difference in the estimated electron density. In comparison, the peak intensity increased by approximately a factor of four. As Stark broadening was much more sensitive to the electron density than the electron temperature [18], this result suggested that the increase in the emission intensity could be caused by an increase in the electron energy. This result may also contribute to the trend observed in Figure 5. Due to the high ionization energy of water and therefore the difficulty of direct electron impact dissociation, one main dissociation route was through H_2O vibrational excitation followed by dissociative attachment [15]. The vibrational excitation cross-section of water showed an increase with electron temperature followed by a slow decrease [20]. Therefore, a decrease in the dissociation efficiency could be caused by the lower vibrational excitation degree at a high electron temperature.

Another useful plasma parameter that could be obtained easily from the emission spectra was the rotational temperature of the OH ($A^2\Sigma^+$) state. The OH radical is an important oxidative intermediate that contributes to the overall dissociation reaction. Due to the prominence of the A-X emission band near 306 nm, the feature was easily captured in our system and fitted for using numerical simulation. Spectra were captured over a range of discharge power and Ar flow rates. The rotational temperature was then calculated from numerical simulation using methods developed by Izarra [21] but with a two-temperature rotational population distribution. The range of spectra fitted was from 306 to 310 nm, which was almost exclusively occupied by the $(v', v'') = (0, 0)$ rotational manifold. An example of the fitted spectrum is shown in Figure 8. It should be noted that the OH

($A^2\Sigma^+$) rotational population was well-known for following a phenomenological two-temperature distribution in atmospheric plasma because of its many creation modes [22]. A range of conditions were studied here, including discharge powers between 3 and 5 W at 40 sccm and flow rates from 100 to 700 sccm at 2.2 W of discharge power. Both the high and low temperatures were almost constant after considering the estimated uncertainty of the simulation. The low temperature was approximately 320 K and the high temperature was approximately 5000 K. The low temperature portion of the population accounted for about 65% of the total population. This suggested that although the efficiencies and dissociation percentage changed within the experiments, the reaction pathway remained the same over these conditions.

CHAPTER 4

CONCLUSIONS

In summary, an Al/Al_2O_3 microchannel plasma device was used to generate H_2 at atmospheric pressure through the dissociation of water vapor with Ar as the carrier gas. The effects of the discharge power and gas flow rate through the device were studied. It was further shown that an optimal flow rate and discharge power existed, whereby the dissociation degree and energy efficiency were maximized. A H_2 generation rate as high as 28 sccm at a production efficiency of 5.8 sccm/W (2.5% energy efficiency) was achieved, which compared favorably to the scientific literature. Furthermore, optical emission studies of the plasma showed that the electron density in the device was ~ $1.5 \times 10^{16}/cm^3$ and varied little at discharge powers close to the power level that resulted in the highest dissociation energy efficiency. In addition, fitting to the OH (A-X) emission spectra revealed the non-equilibrium nature of the OH (A) intermediate. Microchannel plasma devices were shown here to be suitable for H_2 generation as compared with other plasmachemical devices.

FIGURES

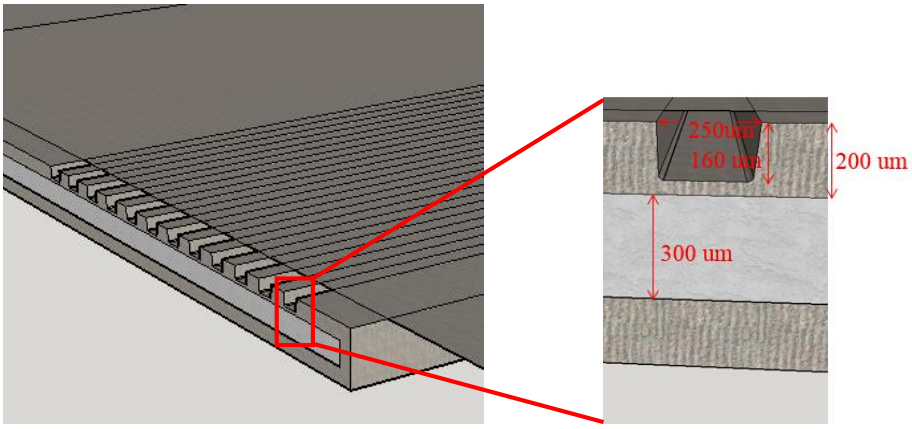

Figure 1. Cross sections of the microchannel plasma reactors. Both the top and bottom plates were anodized to form an Al/Al_2O_3 structure. The striped slate regions represent the porous alumina sections. The grey regions represent the aluminum sections.

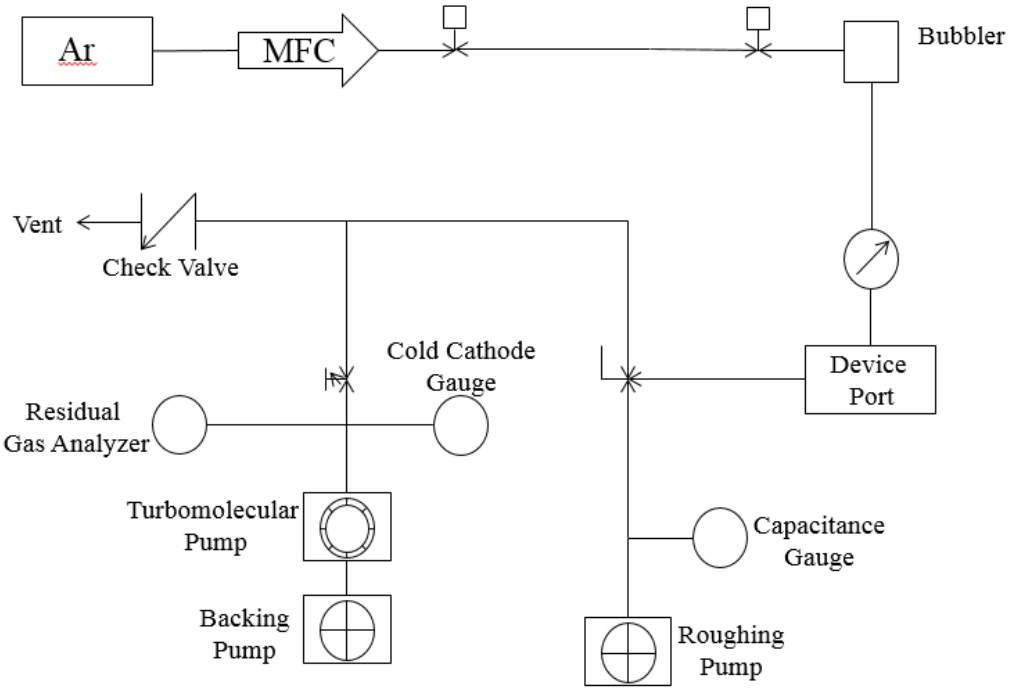

Figure 2. Gas flow and testing system setup. Water was carried into the device through a bubbler. The resulting gas was assumed to be saturated with water vapor.

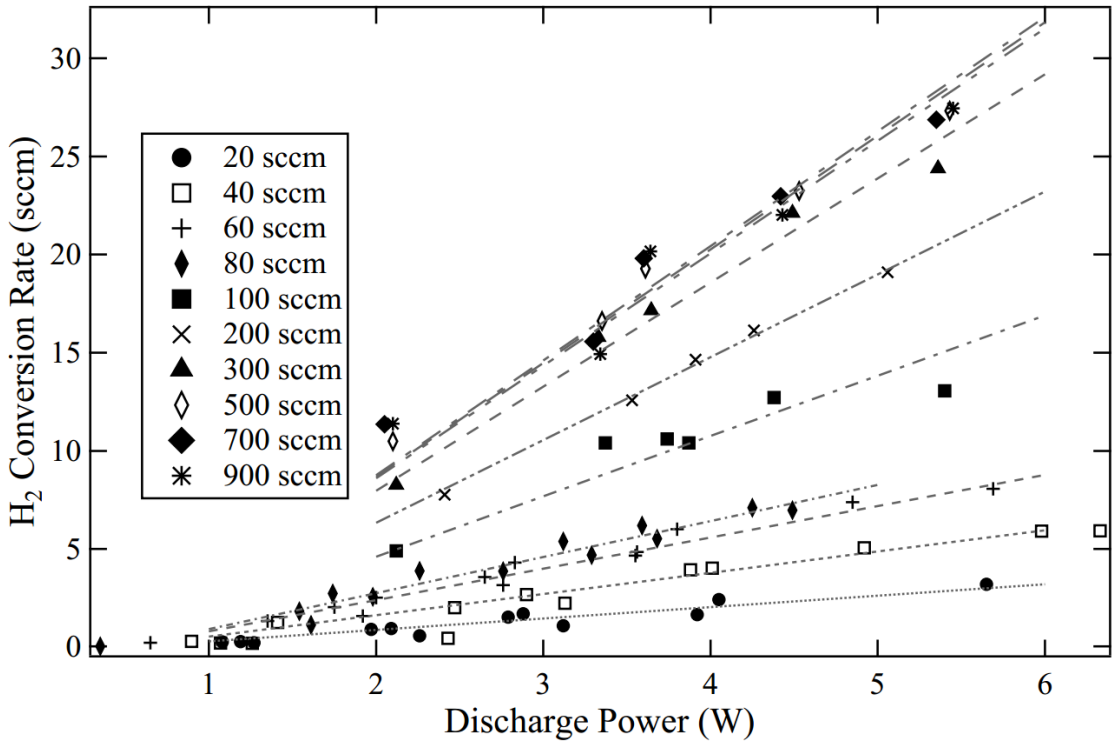

Figure 3. Absolute H_2 generation rate as a function of discharge power at various Ar flow rates with linear fits. The data were taken from 10 different plasma devices.

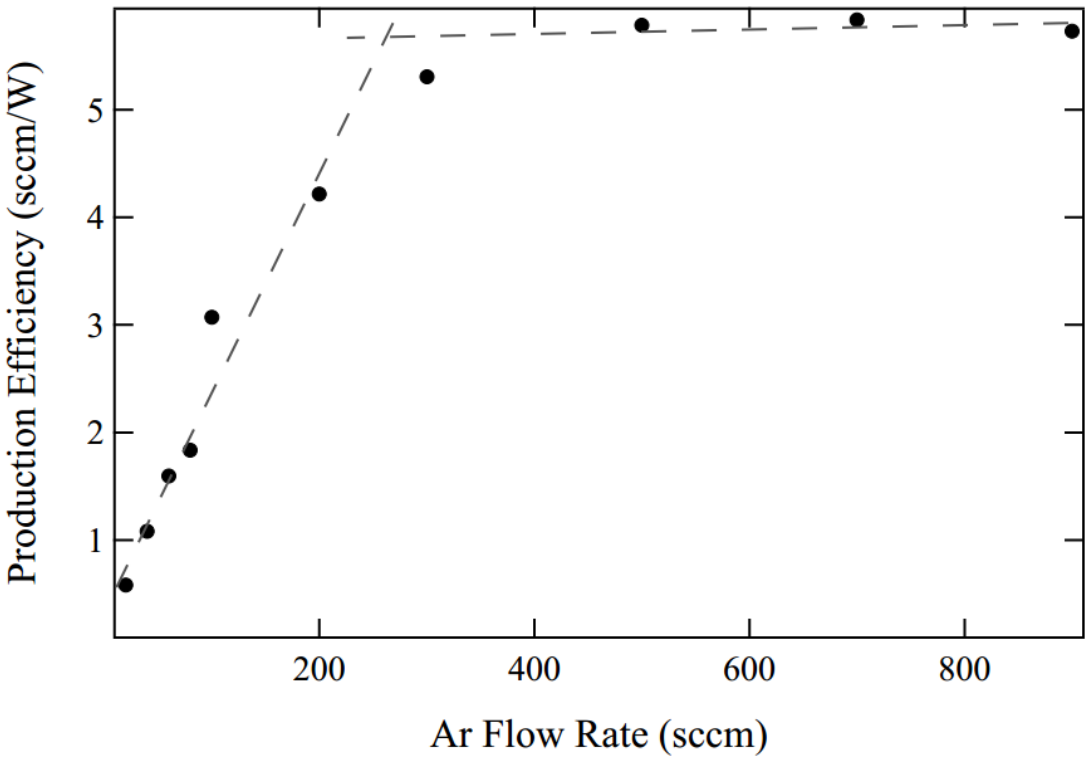

Figure 4. H_2 production efficiency as taken from the slope in Fig. 1 at various Ar flow rates. The production efficiency at low flow rates showed a linear increase with flow rate, but started to saturate at high flow rates above ~400 sccm.

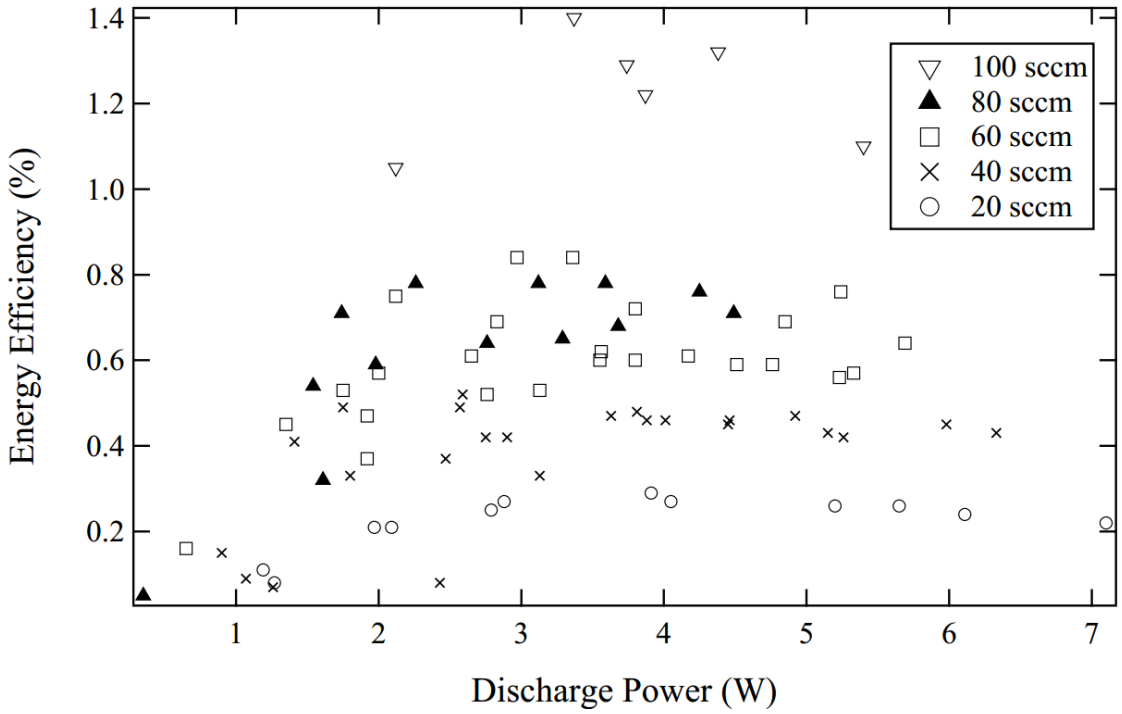

Figure 5. H_2 production energy efficiency taken from 10 different plasma-chemical devices at flow rates between 20 and 100 sccm. The energy efficiency gradually increased at low discharge power and showed maxima at a discharge power of about 4 W.

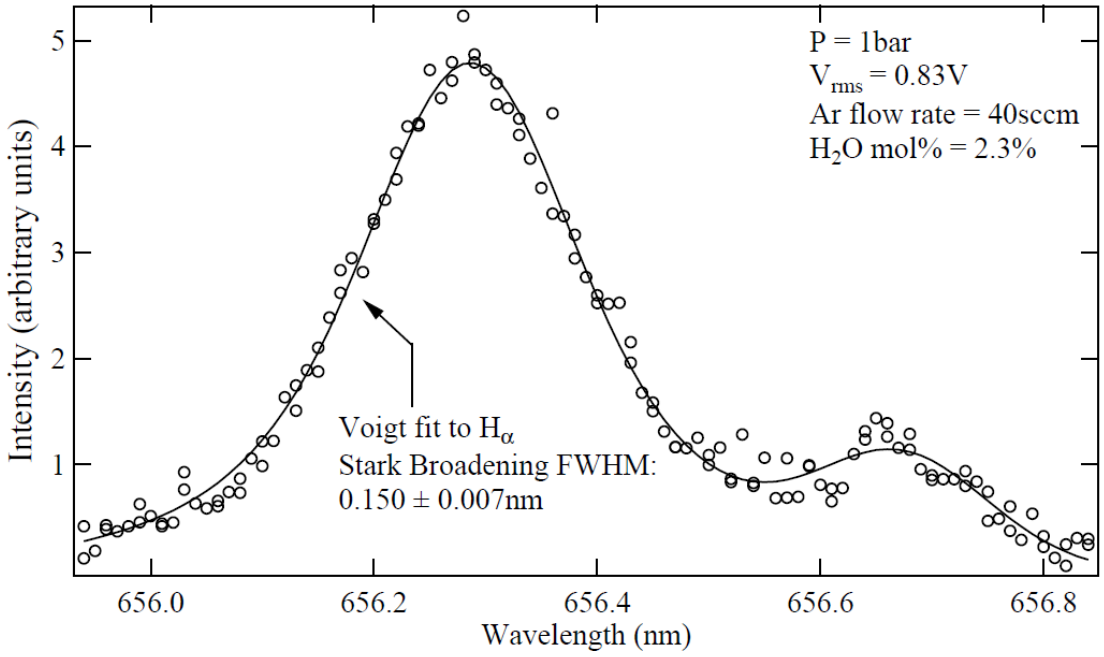

Figure 6. Voigt fit to the H_α line. The value of Stark broadening was extracted from the Gaussian component and correlated to the electron density value based on the model developed in Ref. 18.

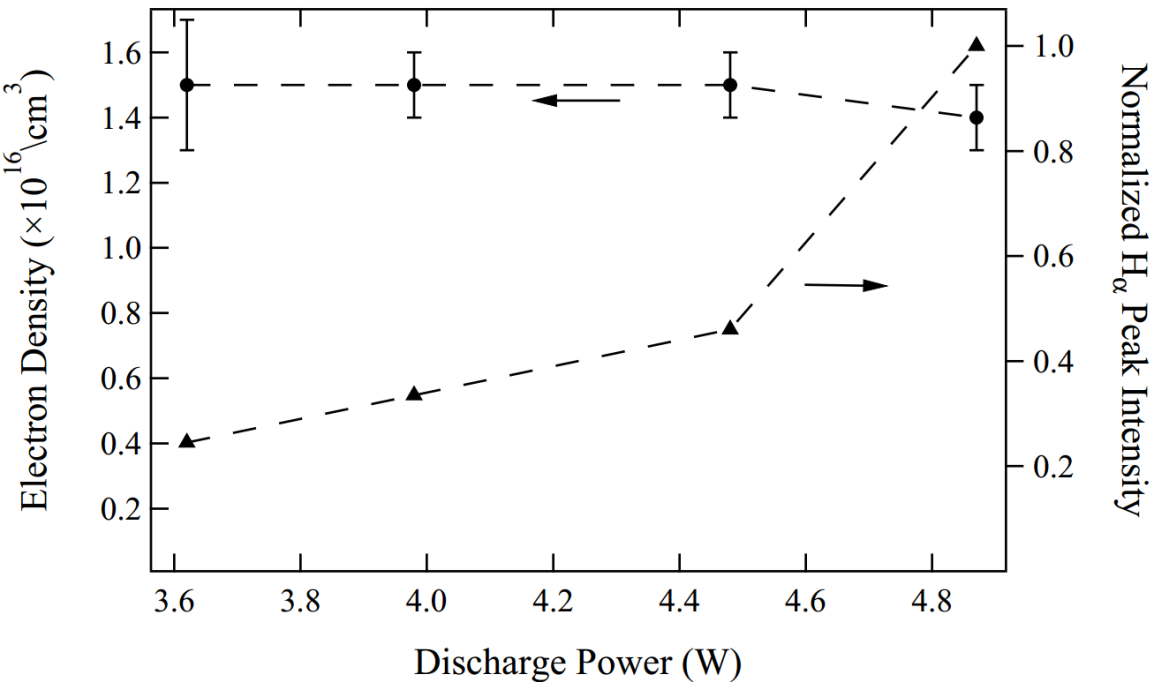

Figure 7. Electron density calculated from Stark broadening as a function of discharge power. The normalized H_α peak intensity is overlaid on top of the raw data. The electron density value showed little change at the measured discharge powers, while the peak intensity underwent a four-fold increase. The error bars represent the uncertainties resulting from the fitting parameter to Stark broadening.

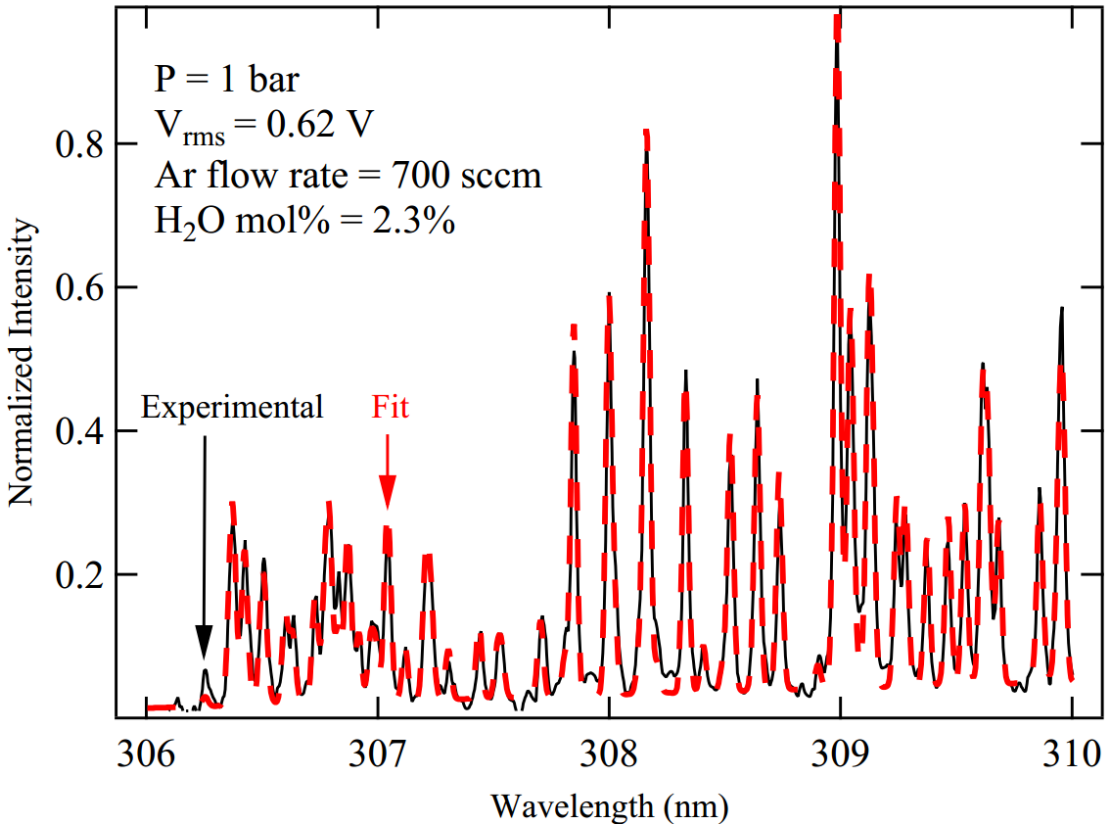

Figure 8. Emission spectrum of OH (A-X) transition around 308 nm. The spectrum was fitted to a non-equilibrium rotational temperature distribution. The fitted low temperature was 339 ± 8 K and accounted for 60.2 ± 0.8% of the population. The fitted high temperature was 4200 ± 200 K.

REFERENCES

[1] T. N. Veziroğlu, "Hydrogen technology for energy needs of human settlements," *Int. J. Hydrogen Energy*, vol. 12, no. 2, pp. 99–129, 1987.

[2] N. Z. Muradov and T. N. Veziroğlu, "'Green' path from fossil-based to hydrogen economy: An overview of carbon-neutral technologies," *International Journal of Hydrogen Energy*, vol. 33, no. 23. pp. 6804–6839, Dec. 2008.

[3] A. P. Simpson and A. E. Lutz, "Exergy analysis of hydrogen production via steam methane reforming," *Int. J. Hydrogen Energy*, vol. 32, no. 18, pp. 4811–4820, Dec. 2007.

[4] R. Asisov, A. Vakar, A. Gustol, V. Givotov, E. Krasheninnikov, M. Krotov, V. Rusanov, A. Fridman, and G. Sholin, "Plasmachemical methods of energy carrier production," *International Journal of Hydrogen Energy*, vol. 10, no. 7. pp. 475–477, 1985.

[5] J. H. Chaffin, S. M. Bobbio, H. I. Inyang, and L. Kaanagbara, "Hydrogen production by plasma electrolysis," *Journal of Energy Engineering*, vol. 132, no. 3. pp. 104–108, Dec. 2006.

[6] X. Chen, S. L. Suib, Y. Hayashi, and H. Matsumoto, "H_2O splitting in tubular PACT (plasma and catalyst integrated technologies) reactors," *J. Catal.*, vol. 201, no. 2, pp. 198–205, Jul. 2001.

[7] S. L. Suib, Y. Hayashi, and H. Matsumoto, "Water splitting in low-temperature AC plasmas at atmospheric pressure," *Res. Chem. Intermed.*, vol. 26, no. 9, pp. 849–874, 2000.

[8] H. Kabashima, H. Einaga, and S. Futamura, "Hydrogen generation from water with nonthermal plasma," *Chem. Lett.*, vol. 30, no. 12, pp. 1314–1315, 2001.

[9] S. V. T. Nguyen, J. E. Foster, and A. D. Gallimore, "Operating a radio-frequency plasma source on water vapor," *Rev. Sci. Instrum.*, vol. 80, no. 8, p. 083503, Aug. 2009.

[10] M. H. Kim, J. H. Cho, S. B. Ban, R. Y. Choi, E. J. Kwon, S.-J. Park, and J. G. Eden, "Efficient generation of ozone in arrays of microchannel plasmas," *J. Phys. D. Appl. Phys.*, vol. 46, no. 30, p. 305201, Jul. 2013.

[11] J. H. Cho, S.-J. Park, and J. G. Eden, "Propagation and decay of low temperature plasma packets in arrays of dielectric microchannels," *Appl. Phys. Lett.*, vol. 101, no. 25, p. 253508, 2012.

[12] S. H. Sung, I. C. Hwang, S.-J. Park, and J. G. Eden, "Interchannel optical coupling within arrays of linear microplasmas generated in 25–200μm wide glass channels," *Appl. Phys. Lett.*, vol. 97, no. 23, p. 231502, 2010.

[13] C. Hibert, I. Gaurand, O. Motret, and J. M. Pouvesle, "[OH(X)] measurements by resonant absorption spectroscopy in a pulsed dielectric barrier discharge," *J. Appl. Phys.*, vol. 85, no. 10, p. 7070, 1999.

[14] F. Rehman, J. H. Lozano-Parada, and W. B. Zimmerman, "A kinetic model for H2 production by plasmolysis of water vapours at atmospheric pressure in a dielectric barrier discharge microchannel reactor," *Int. J. Hydrogen Energy*, vol. 37, no. 23, pp. 17678–17690, Dec. 2012.

[15] A. Fridman, *Plasma Chemistry*. Cambridge University Press, 2008.

[16] Q. Wang, I. Koleva, V. M. Donnelly, and D. J. Economou, "Spatially resolved diagnostics of an atmospheric pressure direct current helium microplasma," *J. Phys. D. Appl. Phys.*, vol. 38, no. 11, pp. 1690–1697, Jun. 2005.

[17] J. Muñoz, M. S. Dimitrijević, C. Yubero, and M. D. Calzada, "Using the van der Waals broadening of spectral atomic lines to measure the gas temperature of an argon–helium microwave plasma at atmospheric pressure," *Spectrochim. Acta Part B At. Spectrosc.*, vol. 64, no. 2, pp. 167–172, Feb. 2009.

[18] M. A. Gigosos, M. A. González, and V. Cardeñoso, "Computer simulated Balmer-alpha, -beta and -gamma Stark line profiles for non-equilibrium plasmas diagnostics," *Spectrochimica Acta - Part B Atomic Spectroscopy*, vol. 58, no. 8, pp. 1489–1504, 2003.

[19] D. Yarmolich, Y. E. Krasik, E. Stambulchik, V. Bernshtam, J. K. Yoon, B. Herrera, S.-J. Park, and J. G. Eden, "Self-pulsing 10^4 A cm^{-2} current density discharges in dielectric barrier Al/Al_2O_3 microplasma devices," *Appl. Phys. Lett.*, vol. 94, no. 1, p. 011501, 2009.

[20] Y. Itikawa and N. Mason, "Cross sections for electron collisions with water molecules," *J. Phys. Chem. Ref. Data*, vol. 34, no. 1, pp. 1–22, 2005.

[21] C. De Izarra, "UV OH spectrum used as a molecular pyrometer," *J. Phys. D. Appl. Phys.*, vol. 33, no. 14, pp. 1697–1704, 2000.

[22] P. Bruggeman, D. Schram, M. Á. González, R. Rego, M. G. Kong, and C. Leys, "Characterization of a direct dc-excited discharge in water by optical emission spectroscopy," *Plasma Sources Sci. Technol.*, vol. 18, no. 2, p. 025017, May 2009.